Journal of Fluids and Structures 18 (2003) 305–324

JOURNAL OF FLUIDS AND STRUCTURES

www.elsevier.nl/locate/jnlabr/yjfls

Force coefficients and Strouhal numbers of four cylinders in cross flow

K. Lam[a,*], J.Y. Li[b], R.M.C. So[a]

[a] *Department of Mechanical Engineering, The Hong Kong Polytechnic University, Hung Hom, Kowloon, Hong Kong*
[b] *Department of Fluid Engineering, Xi'an Jiaotong University, Shaanxi, People's Republic of China*

Received 30 September 2002; accepted 28 July 2003

Abstract

This paper presents the measurements of force coefficients and Strouhal numbers (St) on four cylinders in a square configuration at subcritical Reynolds numbers (Re) using a piezo-electric load cell in a wind tunnel. Six spacing ratios (L/D) varying from 1.69 to 3.83 and 13 angles of incidence α ranging from 0° to 180° at a 15° interval covering all orientations were investigated. With the help of a laser-induced fluorescence visualization technique, it is found that the variation of forces and Strouhal numbers with L/D are governed by three distinct flow patterns. They are: (a) free oscillations of shear layers and vortex formation at large L/D; (b) reattachment of shear layer or shielding flow for intermediate L/D and (c) narrow gap flows for small L/D. Two major causes for large fluctuating forces are discussed in this paper and the force results are compared with other measurements. It is concluded that the flow patterns, i.e., the development and the interferences of the free shear layers and the distribution of the wake vortices of the cylinders play a key role in the variation of the forces and shedding frequencies. Consequently, the downstream cylinders are usually subjected to more serious fluctuating forces under the influence of unsteady wake vortices. Also, the upstream cylinders normally experience larger mean drags than the downstream ones.

1. Introduction

It is a well-known phenomenon that when a single bluff body or a bundle of bluff bodies are subjected to a cross flow, vortex shedding from the structure would induce fluid excitation forces which, in turn, lead to flow-induced vibration. Although flow-induced vibration is governed by a number of major parameters, such as Reynolds number (Re), effective damping ratio, mass ratio, etc., the forces including the mean forces, the fluctuating forces and their associated fluctuating frequencies play a very important role in flow-induced vibration. The resulting vibration has significant impact on the fatigue life of structures and could cause disastrous failure of industrial facilities with heavy financial losses and even loss of human lives. Therefore, engineers and scientists have spent much effort to investigate the fluctuating forces and the vortex shedding characteristics of cylindrical structures (see, e.g., Newman and Karniadakis, 1997; Sakamoto and Haniu, 1994).

In general, several mechanisms will give rise to flow-induced vibration. The most frequently encountered are those due to vortex shedding, turbulent buffeting, fluidelastic instability and acoustic resonance (Paidoussis, 1982; Fitzpatrick et al., 1988; Price and Zahn 1991; Oengoren and Ziada, 1998). Any bluff body exposed to a cross flow may experience one or more of these mechanisms. Due to the complexity of flow separation and free shear layers interaction of bluff bodies, the mechanism of fluid excitation forces and their related frequencies is a highly nonlinear phenomenon.

*Corresponding author. Tel.: +852-27666649; fax: +852-2365470.
E-mail address: mmklam@polyu.edu.hk (K. Lam).

0889-9746/$ - see front matter © 2003 Elsevier Ltd. All rights reserved.
doi:10.1016/j.jfluidstructs.2003.07.008

Circular cylinders, being a typical example of bluff bodies, such as those found in power transmission lines, heat exchangers in nuclear power plants, offshore structures, suspension bridges, etc., are the most widely used bluff bodies in industry. Therefore, studies on a circular cylinder or an array of circular cylinders have attracted much more attention, compared with other types of bluff bodies, and are of great importance both in fluid dynamics theory and engineering applications.

Studies on a single circular cylinder in a cross flow have been carried out most extensively and insight into the mechanisms of flow-induced vibration has been gained by studying the force characteristics due to various situations of fluid–structure interactions. For example, So and Savkar (1981) measured the spanwise averaged steady and unsteady forces induced by a uniform or turbulent cross flow over a smooth circular cylinder using static pressure taps, piezo-electric three-axis load cells and a hot film. The parameters examined in their experiment included Re, ranging from 2×10^4 to 2×10^6, the free-stream turbulence intensity, the integral length scale-to-diameter ratio and the active span-to-diameter ratio. On the other hand, Sin and So (1987) measured the induced local unsteady forces acting on cylinders placed in a cross flow using the same techniques. In addition, simultaneous measurements of the flow-induced local unsteady forces on the cylinder and the stream velocity in the wake were carried out by Baban and So (1991a, b). These results together with mean drag measurements along the span and available literature data were used to evaluate the flow mechanisms responsible for the induced unsteady forces and the effect of aspect ratio on these forces. The above experiments (Baban and So, 1991a, b) were conducted at a cylinder $\mathrm{Re}=46{,}000$ using three finite-span cylinders with span-to-diameter ratios of 2, 1.5 and 1, respectively.

Besides the work mentioned above, efforts have also been made on similar aspects of cross flow around a single cylinder using different experimental set up. For example, Schewe (1983) conducted force measurements in a pressurized wind tunnel from subcritical up to trans-critical Re (2.3×10^4 to 7.1×10^4) without changing the experimental arrangement. The steady and unsteady forces and the Strouhal frequencies were measured by means of a piezobalance (assembly of three-component load piezo-electric force-measuring elements). In the critical Re range, two discontinuous transitions that could be interpreted as bifurcations at two critical Reynolds numbers were found. West and Apelt (1993, 1997) performed another important experiment on the force measurements of a single cylinder in a cross flow. The root mean square (rms) lift and drag forces in subcritical flow (1×10^4 to 2.5×10^5) on an elemental slice of the cylinder were established using accurate measurements of the fluctuating pressure distribution. The spanwise cross-correlation of the fluctuating pressure and the elemental fluctuating forces were presented, including the effects of the variation of Re, aspect ratio, free stream turbulence and wind tunnel blockage. Other interesting investigations, such as Fox and West (1993a–c), Szepessy and Bearman (1992) and Blackburn and Melbourne (1996), have also been carried out. Apart from the experimental investigations, continuous efforts on numerical methods have been pursued and detailed information about the different mechanisms of flow-induced vibration has been obtained (So et al., 2001; Blackburn and Henderson, 1999; Freitas, 1995).

The variation of the forces and Strouhal frequencies are further complicated by the presence of neighboring cylinders. The forces and shedding frequencies would also vary greatly with changes in the ratio of the center-to-center cylinder spacing L to their diameter D, the orientation of the cylinder array and the number of cylinders, in addition to the characteristic parameters mentioned above. Therefore, the nonlinear interactions between two cylinders or among multiple cylinders are far more complicated than the flow-induced vibration phenomena given rise by a single cylinder. These interaction phenomena have been widely investigated because of their inherent importance and practical significance in many branches of engineering.

The interference between two cylinders, being the simplest example of an array of cylinders, has drawn considerable attention in the past. To cite a few examples, Price and Paidoussis (1984) experimentally investigated the mean lift and drag forces acting on two and three cylinders over a wide range of L/D and suggested that the principle of superposition could apply in the determination of force coefficients. Zdravkovich (1987) proposed to classify the flow interference between two cylinders into three categories after completing a comprehensive review of numerous experimental investigations on two cylinders in a cross flow and has drawn a map of mean force coefficients and Strouhal number (St) for two cylinders in the subcritical Re regime. On the other hand, Ting et al. (1998) employed both pressure and force measurement techniques to measure the fluid-elastic forces on one of two staggered circular cylinders over a wide range of configuration and Re. Besides the force measurements cited above, other investigations on fluid–structure interaction between two cylinders and their effect on flow pattern, flow field, bistable flow and related variation of St have also been carried out (Kim and Durbin, 1988; Sumner et al., 1999, 2000).

It has now been realized that the principle of superposition cannot be applied to the highly nonlinear situation of cross flow around cylinders; therefore, only a few papers have reported on multi-cylinder arrays compared with numerous papers published on two cylinders and one cylinder. Even among the papers on multi-cylinders, many of them were on multi-cylinders in line, side-by-side or in tandem (Guillaume and LaRue, 1999; Kareem et al., 1998). The investigation of Lam and Cheung (1988) on three cylinders in an equilateral arrangement, on the other hand, clearly

showed that some well-known flow patterns in two-cylinder arrays have been significantly changed owing to the presence of a third cylinder. Hence, work on the mechanism of flow-induced vibration and the overall flow patterns around multi-cylinder arrays need further exploration.

A four-cylinder array in a square configuration is a basic unit in multi-cylinder arrays and tube banks. The study of four-cylinder arrays would be helpful to the understanding of the flow physics, of the flow interaction mechanisms and of the force characteristics of the more complicated flow in much larger cylinder arrays, which are specially evident for the cases of in-line square and rotated square arrangements in heat exchanger tube banks. It also has many direct practical applications, such as in offshore structures. Nevertheless, investigation on this simple cylinder array is still rather scarce and has not been well documented in the literature. The flow visualization results of Lam and Lo (1992) and Lam et al. (2003) revealed that flow around the four cylinders in a square configuration is far more complicated than that in one or two cylinders. Using a pressure method to measure force, the experiments (Sayers, 1988, 1990; Lam and Fang, 1995) on four cylinders at $\mathrm{Re} = 3 \times 10^4$ and 1.28×10^4 revealed that the magnitude of the mean lift and drag coefficient is strongly influenced by the orientation of the array group to the free stream. At certain L/D and α, asymmetrical vortex shedding occurs, while in other situations, vortex shedding behind certain cylinders may be completely absent. In addition, Farrant et al. (2000) and Lam et al. (2001) attempted to simulate the flow around four cylinders in a square configuration at small and subcritical Re and at two different α using cell boundary element and surface vorticity method, respectively. However, their attempts cannot reproduce the flow patterns as obtained in experiments at certain L/D and α. Furthermore, important questions remain unanswered. For example, the fluctuating forces acting on the four cylinders, though they are the primary forces in flow-induced vibration, have not been measured systematically. Hence, the first question is how these fluctuating forces and shedding frequencies will change with different flow patterns? How will the mean and fluctuating forces vary at different α and L/D? Are the mean force characteristics obtained by pressure integration at mid-span similar to those deduced from direct spanwise averaged measurements using a load cell? Is the St obtained by counting vortices in flow visualization study, such as that carried out by Lam and Lo (1992), equivalent to the St determined from spectral analysis of the measured fluctuating forces? These and other less important questions need addressing if fluid–structure interaction of multiple-cylinder arrays in a cross flow were to be understood.

In an attempt to answer some of the above questions, the present work aims to experimentally investigate the forces acting on four cylinders in a square configuration, including the mean and fluctuating force, and the St. A load cell is used to measure the spanwise averaged force acting on the cylinders and the experiments are carried out in a close circuit wind tunnel. Therefore, the forces acting on the cylinders have relatively small magnitude and an extremely sensitive force transducer with a suitable dynamic range is required to correctly resolve the fluctuating forces. The experiments are carried out in the L/D range of 1.69–3.83 at a 0.43 interval and a α range of 0°–180° at a 15° interval. It is hoped that these studies could provide a useful database and a penetrative understanding of the physics of fluid–structure interaction of multiple-cylinder arrays in a cross flow.

2. Experimental arrangement and calibration

2.1. Wind tunnel

The experiments were conducted in a closed circuit low-speed wind tunnel with a cross-section of 0.6 m × 0.6 m and a 2 m long test section. The walls of the test section are made of Perspex to facilitate cylinder model installation and flow observation. The velocity in the test section is uniform and could be continuously varied up to 40 m/s using a speed controller. The thickness of the boundary layer at the test location is about 20 mm while the free stream turbulent intensity is estimated to be less than 0.2%. During the experiment, a standard Pitot-static tube was used to monitor the wind speed and the pressure was read using an electronic micro-manometer made by Furness Control Limited. The temperature in the wind tunnel was kept constant by regulating the air temperature in the laboratory.

2.2. The cylinder models

In this experiment, the free-stream velocity is in the x direction, which is also the positive drag direction, while the positive lift is in the y direction. Among the four cylinders arranged in a square configuration, only one of them was instrumented and the forces on it were measured directly by a load cell. A schematic diagram of the array configuration is shown in Fig. 1. The incident angle β was measured with respect to the diagonal of the instrumented cylinder and its counterpart on the opposite corner, i.e., the diagonal joining cylinders 1 and 3. On the other hand, the angle of attack α was measured with respect to the line joining the center of cylinders 1 and 4 and referred to as array angle when the

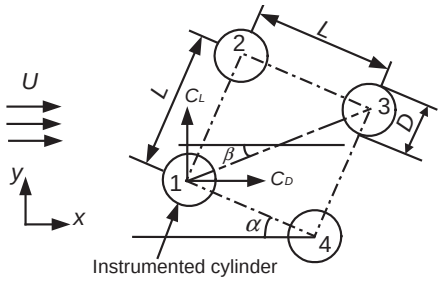

Fig. 1. A schematic layout of the four-cylinder array.

Table 1
The relationship between array attack angle α and cylinder incident angle β

Array attack angle α (deg)	Cylinder number	Cylinder incident angle β (deg)
0	Cylinder 1	45
	Cylinder 2	−45
	Cylinder 3	−135
	Cylinder 4	135
15	Cylinder 1	30
	Cylinder 2	−60
	Cylinder 3	−150
	Cylinder 4	120
30	Cylinder 1	15
	Cylinder 2	−75
	Cylinder 3	−165
	Cylinder 4	105
45	Cylinder 1	0
	Cylinder 2	−90
	Cylinder 3	180
	Cylinder 4	90

cylinders were considered as an array group. Therefore, as cylinder 1 rotates from one corner to another, β varies and the change depends on α. The change of β with respect to α is given in Table 1.

All the cylinders were made of hollow brass tubes. One end of each tube was sealed with a flat brass cap while the other end was fitted with an adapter cap. The outer diameters of the cylinders were 35 mm. The cylinders spanned across the length of the test section and this led to an aspect ratio of about 17 and a blockage ratio (per cylinder) of 5.8%. The single cylinder aspect ratio is larger than but the blockage ratio is less than those reported on one cylinder by other investigators; a summary comparison is given in Baban et al. (1989). The projected area blocking the oncoming flow is constant for a square configuration; therefore, the total blockage in the present setup is 11.6%. This blockage falls within the single cylinder blockage reported in West and Apelt (1982) and Schewe (1983), and less than the experimental setup of Richter and Naudascher (1976). In the experiments of West and Apelt (1982), they found that the measured mean drag coefficient did not have any significant variation within a blockage range of about 9–15% over an aspect ratio range of 6–8. Nevertheless, it should be borne in mind that blockage does contribute to the noted experimental scatter on the measured mean drag among various studies (Baban et al., 1989). Just as in previous reports, no correction was made in the measured forces to account for blockage in the present results. All four cylinders were installed vertically in a cantilever manner with a clearance of 1–2 mm between the ends of the cylinders and the bottom wall of the test section.

Three normal cylinders were installed vertically on a turntable plate that was flush mounted on the upper wall of the wind tunnel and could be rotated to any desired angle. The ends of the adaptors fitted in the three cylinders went through this turntable plate and were tightened up by nuts and bolts from outside of the test section. Therefore, the

length of the cylinder was about 600 mm. The instrumented cylinder, on the other hand, was installed through a hole of 39 mm diameter on the plate with a load cell installed. The clearance between the hole and the cylinder is about 1–2 mm. The load cell was secured on a rectangular plate with two transverse slots, while this plate was in turn installed on a second bigger rectangular plate with two slots in the streamwise direction. The big rectangular plate was then mounted on the yoke of the wind tunnel. Therefore, the instrumented cylinder could move to any place where the hole was. The length of the instrumented cylinder is about 640 mm. A schematic diagram of the array installation is shown in Fig. 2.

The spacing ratio, L/D, is defined as the center-to-center distance of adjacent cylinders divided by the cylinder diameter as shown in Fig. 1. On the turntable disc, there were different patterns of holes arranged at different distances, corresponding to different L/D of the cylinders. The maximum L is 134 mm, corresponding to $L/D = 3.83$, while the minimum L is 59 mm, corresponding to $L/D = 1.69$. Between these two limits, seven equi-spaced holes at 15 mm interval were created. The sidewall proximity effects are insignificant for the present configurations studied, even for the rotated square configuration of $L/D = 3.83$ where the smallest distance between the center of the cylinders and the sidewall of the wind tunnel is 205 mm (or about $5.9D$). Past experience on vortex shedding frequency and flow patterns indicated that $5D$ is enough to minimize proximity effects. This estimation is supported by various numerical simulations which reported computational domains with similar range of transverse distance to the wall. For example, the transverse distance to the wall in the numerical studies of Li et al. (1992) and So et al. (2001) is $5D$, while $7D$ is specified in the work of Tutar and Hold (2001).

2.3. Force measurement and load-cell calibration

A piezo-electric load cell has the advantage of high response, high resolution, high stiffness and can give the integral force directly, therefore, many researchers (e.g. So and Savkar, 1981; Schewe, 1983) used this technique to measure the spanwise averaged mean and fluctuating force acting on a single cylinder. In this study, one Kistler Model 9251A piezo-electric three-axis load cell was used to measure the spanwise averaged forces. The load cell was clamped between two machine-polished stainless steel plates through bolts with a pre-load of approximately 100 kN exerted on the load cell. Since the maximum force on the load cell was far less than 10 kN, the requirement for pre-load-to-measured-load ratio of above 10 was achieved. In fact, this ratio is more than 100 for this series of experiments. Therefore, the signal-to-noise ratio of the measured force is very high. The instrumented cylinder was mounted vertically in the z direction, while the x and y directions of the load cell are in the drag and lift direction, respectively.

Calibration of the load cell was carried out statically using dead weights as shown in Fig. 3. The same weight acting on the beam could produce a decreasing output voltage when the moment arm is increased. In this study, three different weights, 0.2, 0.3 and 0.5 kg, were used. By adjusting the scale coefficients of the charge amplifiers linearly to maintain the output of the load cell to have a constant voltage at the origin, the calibration result thus obtained is shown in Fig. 4. It can be seen that the drop of voltage output for the lift and drag direction changes linearly with the moving of the dead weight along the cylinder span. Therefore, it can be concluded that the linearity of the output voltage with

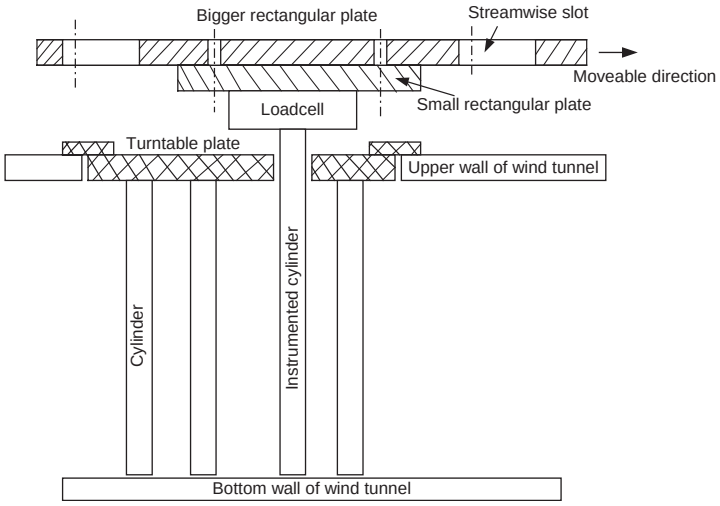

Fig. 2. A schematic assembly of the cylinders in the wind tunnel.

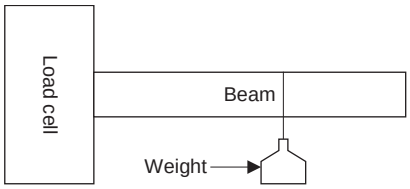

Fig. 3. Device used to calibrate the load cell.

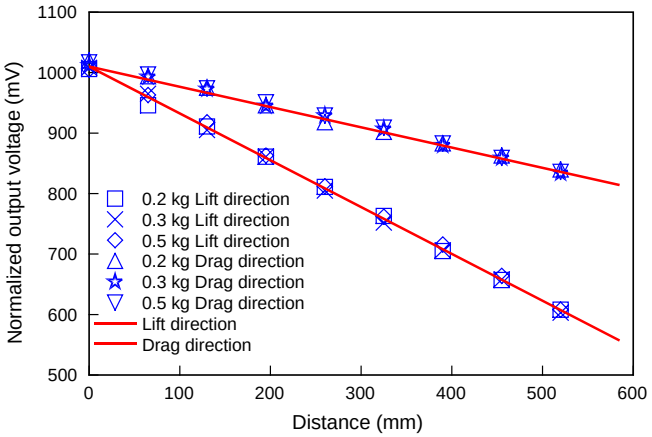

Fig. 4. Linear calibration results in two different directions of the load cell.

weight at one specific location and along the span has been established. Furthermore, the linearity was found to be repeatable. Assuming a uniform distribution of the wind load along the span, the averaged forces acting on the instrumented cylinder can be determined.

2.4. Data recording and processing

A United Electronics Industry (UEI) WIN-30PGSH 12-bit A/D board with 16 analogue input channels was used to record the force signals. The maximum sampling rate is 1000 KHz. The signals from the load cell in its x and y directions were simultaneously measured and low-pass filtered, amplified and then digitized at a sampling rate of 3.33 kHz per channel. They were then transferred to a personal computer through a multiplexer. The duration of each record was about 20 s and the signals were analyzed using a MATLAB program.

2.5. Technique validation on a single cylinder

In order to test the reliability of the measuring system, the forces on a single cylinder and the associated St were measured and compared with the results published in the literature. The force results are shown in Table 2. The Strouhal number St = 0.205 was obtained by analyzing the spectrum of the fluctuating lift force. It is in good agreement with the generally reported value in the subcritical Re range (So and Savkar, 1981; Schewe, 1983). The measured mean drag coefficient (C_D) agrees well with the results of Schewe (1983) who reported a $C_D = 1.22$ in this range. Among the reported measured root mean square fluctuating lift force coefficient C'_L, its value ranges from a low of 0.22 (Tadrist et al., 1990) to a high of about 1 (Richter and Naudascher, 1976; So and Savkar, 1981). Different techniques have been used to measure the fluctuating forces; these include piezo-electric load cells (Richter and Naudascher, 1976; So and Savkar, 1981), load balance composed of piezo-electric load cells (Schewe, 1983) and miniature pressure transducers (West and Apelt, 1997). The load balance gives a low value, while the pressure transducers yield values that are in between those obtained from load balance and direct load cell measurements. The present measurements are closest to those reported by Schewe (1983). In the experiment of Tadrist et al. (1990), they noted that many factors, such as aspect ratio, blockage, turbulence intensity, tube end boundaries, etc., could have great influence on the measured fluctuating

Table 2
Load cell measured forces on a single circular cylinder

Re	C_D	C'_L	C'_D
4.8×10^4	1.186	0.138	0.089
5.4×10^4	1.218	0.217	0.091
6.0×10^4	1.217	0.274	0.133

forces. Therefore, the large difference between the blockage ratio (5.8% vs. 10%) and aspect ratio (17 vs. 10) of the present experiment and that of Schewe (1983) might be the major reasons for the noted discrepancy. According to the experiments of West and Apelt (1997), at similar blockage and aspect ratio, the measured results for C'_L and the root mean square fluctuating drag coefficient (C'_D) were approximately at $C'_L = 0.25$ and $C'_D = 0.06$, which are in fair agreement with the present results. Therefore, the current measurements are in agreement with reported values and the measuring system can be considered reliable.

Clearance effect between the end of the cylinder and the wind tunnel wall was also assessed in this study. It was found that a clearance of 1 mm could produce a 2–3% higher value in the measured mean drag coefficient than that measured at a clearance of 4 mm. Although the influence of clearance was not very significant, all experiments were carried out with a clearance of 1–2 mm in order to assure consistent force measurements.

In our analysis, the resolution of the FFT results on shedding frequency was 1 Hz, and the forces were allowed to be measured to the nearest 18 mN in the maximum range of −18 to 18 N, so the uncertainty estimates caused by resolution for St was about 1% and less than 1% for all forces. Furthermore, the cross talk between x and y directions of the load cell is less than 1.2%, and the linearity of the output signals is within 1%. These data are specified in the technical data sheet supplied by the company. They agreed reasonably with the static calibration of the load cell carried out in this experiment. Taking other factors into account, such as misalignment, error in oncoming velocity measurement, etc., the error limits in the present experiments were conservatively estimated to be no more than 10% for forces and less than 5% for Strouhal number.

Error bars with 10% uncertainty for all the forces and St are shown in the following figures for certain spacing ratios L/D. Furthermore, the data for a single cylinder chosen as reference in the comparison with the variation of the induced forces and shedding frequencies in the four cylinder arrays are taken to be $C_D = 1.2$, $C'_L = 0.22$, $C'_D = 0.09$ and $\mathrm{St} = 0.2$.

3. Experimental results and analysis

In order to investigate the change of flow patterns, if any, in the subcritical Re range for the flow around these configurations and to check the shedding frequencies and the associated data more conveniently, the experiments were carried out at different free stream velocities and L/D. The free stream velocities were selected as 9.7, 13.8, 18.1 and 22.3 m/s for $L/D = 3.83$ and 3.4, and 9.7, 13.8, 17.7 and 19.4 m/s for other smaller L/D. This leads to $\mathrm{Re} = 2.25 \times 10^4$, 3.2×10^4, 4.2×10^4 and 5.18×10^4, respectively, for the two larger L/D, and $\mathrm{Re} = 2.25 \times 10^4$, 3.2×10^4, 4.1×10^4 and 4.5×10^4, respectively, for other smaller L/D. From the mean force measurements, it is evident that no change of flow patterns occurred; therefore, only the results at 18.1 or 17.7 m/s, i.e., at Re around 4.1×10^4, are shown in all figures where load cell measurements are reported.

With β increasing from 0 to 180° at an interval of 15° in the anti-clockwise direction, the instrumented cylinder would pass the lower half of the plane as shown in Fig. 1. At the symmetric configuration of $\alpha = 0°$ or 45°, the possible flow field could be either corresponding to a symmetric flow or a flopping bi-stable flow. Therefore, the complete force information on the four cylinders at different array angle α could be obtained with β varying from 0° to 180°. The relationship between α and β is summarized in Table 1 for the range of β tested. To provide a systematic and concise description of the results, and to study the effects of interference among the cylinders more clearly and directly, the results are presented according to the array angle α instead of the incident angle β. Accordingly, α was varied from 0° to 45° at a 15° interval, i.e., four different orientations. The data discussed in the following include the mean forces, the fluctuating forces and St and are presented in decreasing L/D.

3.1. In-line square arrangement

At $\alpha = 0°$, the cylinder array is an in-line square arrangement, and it can be regarded as two parallel rows of two-cylinder arrays in tandem. Typical pictures of the flow patterns, which were carried out at $\mathrm{Re} = 200$ and 800 for

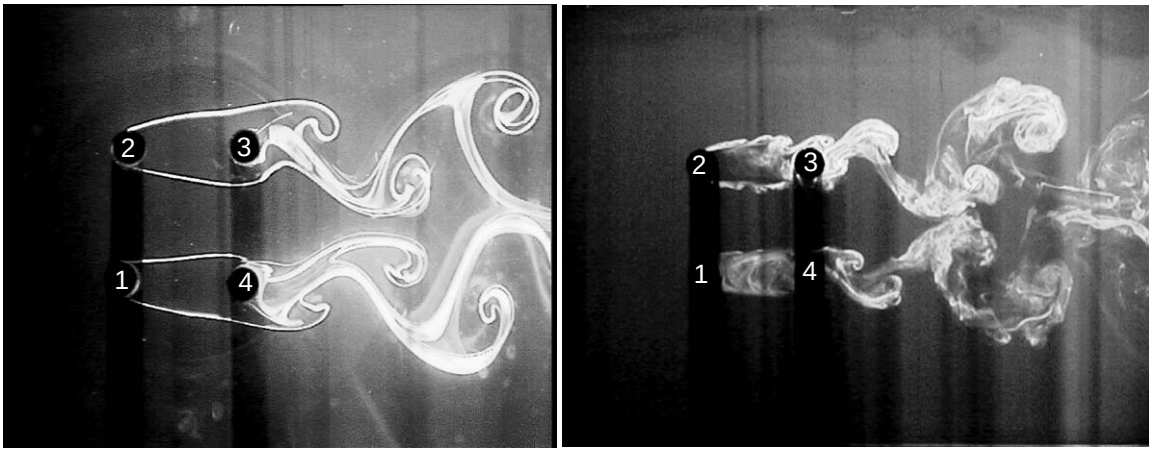

(a) (b)

Fig. 5. Typical flow pattern at $\alpha = 0^\circ$ and $L/D = 4$ in a water tunnel: (a) Re = 200; (b) Re = 800.

$L/D = 4.0$ in a water tunnel, are shown in Fig. 5. The flow visualization experiments were conducted with all four cylinders installed on a circular vertical turntable in a cantilever manner, in a low speed closed-loop water tunnel with a working section of 150 mm × 150 mm. The outer diameter of the cylinder was $d = 10$ mm, which leads to an aspect ratio of about 15 and a blockage ratio (per cylinder) of ~6.7%. These values are similar to those found in the wind tunnel. Each well-polished Plexiglas cylinder has two dye injection holes of 0.5 mm located at mid-span and on opposite sides. The fluorescent dye was Rhodamine for upstream cylinders and Fluorescein for downstream cylinders, respectively. The streak lines were illuminated using a 4W Argon-ion laser, and were recorded with a JVC GY-DV500 Camcorder. Detailed description about the water tunnel and the facilities is given in Lam et al. (2003). From the flow visualization, it can be found that below certain critical L/D, which would change with Re, the downstream cylinders were always in the shadow of the upstream cylinders. Vortex shedding only occurred behind the downstream cylinders, i.e., cylinders 3 and 4.

Reviewing the flow phenomena of two cylinders in tandem would be useful to the understanding of the in-line square arrangement at $\alpha = 0^\circ$. As investigated and generalized by Zdravkovich (1987) and Igarashi (1981), two cylinders in tandem would experience three major flow regimes with decreasing L/D. At large L/D, normally >4.0, the separated shear layer would roll up alternately and form vortices behind the upstream cylinder. Immersed in the wake of the upstream cylinder and impinged by the oncoming vortices, the vortex formation length of the downstream cylinder would be much shorter and two turbulent vortices would form behind it. Therefore, the drag force on the upstream cylinder is larger than that on the downstream cylinder. On the other hand, it is expected that the fluctuating forces on the downstream cylinder are greater than those acting on the upstream cylinder. This is one major mechanism for generating large fluctuating forces. The fluctuating lift force of both cylinders would exhibit a distinct frequency identical to the shedding frequency but the downstream one would also show a second harmonic of the shedding frequency.

For $2.1 < L/D < 3.0$ and dependent on Re, the free shear layer separated from the upstream cylinder would shield or reattach on the downstream one. Therefore, an almost stationary wake region would form in between them and the wake vortices are only formed behind the downstream cylinder. Such flow pattern would lead to a sharp decrease of the fluctuating lift force on both the up- and down-stream cylinder while the vortex shedding frequency of the upstream cylinder would approach zero. With $L/D < 2.1$, the downstream cylinder is immersed in the wake of the upstream one. The immersion is so deep that the vortex shedding behind the downstream cylinder is actually formed by the free shear layer detached from the upstream cylinder.

As for the flow around four cylinders in an in-line arrangement, the overall flow pattern is similar to the flow around two cylinders in tandem at intermediate and large L/D because the interference between the up- and down-stream cylinders is the major mechanism. With L/D decreasing further, the interference arising from the side-by-side cylinders becomes more and more pronounce and the repulsive force becomes larger and larger. According to Lam and Lo (1992), for a square cylinder array at $L/D < 1.7$, a bi-stable state of the wide and narrow wake attached behind cylinders 3 and 4 occurred. On the other hand, for a two side-by-side cylinder array, this phenomenon would occur at $L/D = 1.5-2.0$. Therefore, this difference could be attributed to the presence of the upstream cylinders. From the flow

visualization experiments, it was observed that the interference between two cylinders in tandem would be much more severe than that between their side-by-side counterpart at and above intermediate L/D, while the interference would become quite severe among all four cylinders at small L/D.

The St was determined from spectral analysis of the fluctuating forces using a power spectral density (PSD) plot. At $\alpha = 0°$, cylinders 1 and 4 and cylinders 2 and 3 are symmetrical about the horizontal bisector (two rows form a mirror image of each other), therefore, only the measured results on cylinders 1 and 4 are presented here because what is true for cylinders 1 and 4 is also true for cylinders 2 and 3. Two typical normalized PSD plots, with different scales for the fluctuating lift force of cylinders 1 and 4 at $L/D = 2.54$ and at the same oncoming velocity, are shown in Fig. 6. It is obvious that the spectral peak of cylinder 1 is small and weak while that of cylinder 4 is large and strong. Similar PSD plots were obtained for the fluctuating forces for other L/D, but they are not shown to avoid repetition. All St results were inferred from these PSD plots.

Fig. 7 shows the variation of St vs. L/D. The St of cylinder 4 is around 0.2 for all L/D measured. In addition, the second harmonic shedding frequency was also detected, thus indicating that vortex shedding persists behind cylinder 4 throughout this L/D range. However, for cylinder 1, a distinct shedding frequency is clearly discernible at $L/D = 3.83$; while at $L/D = 3.4$, the peak becomes rather obscure but is still identifiable. Further decrease in L/D gives rise to essentially unidentifiable peaks at L/D=2.97, 2.54 and 2.11, thus St at these L/D vanishes. This represents indirect but clear evidence that vortex shedding from cylinder 1 ceases and the flow phenomenon of shear layer reattachment or downstream cylinder being in the shadow of the upstream cylinder occurs. With L/D decreasing further, a narrow and prominent sharp peak appears again in the lift force PSD plot at $L/D = 1.69$. The St thus determined is very close to that obtained for cylinder 4 (Fig. 7). This could be attributed to the fact that when the upstream and downstream cylinders are so close to each other, the effect of vortex shedding from cylinder 1 is 'felt' by the downstream cylinder. Comparing with the experimental results of Lam and Lo (1992), it is interesting to note that their St showed that vortex

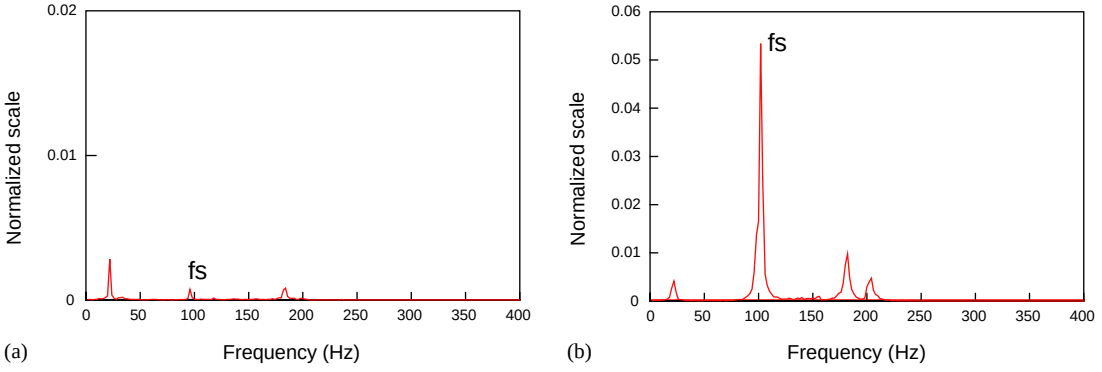

Fig. 6. Normalized power spectral density (PSD) of the fluctuating lift force vs. frequency at $\alpha = 0°$ and $L/D = 2.54$: (a) PSD of cylinder 1 and (b) PSD of cylinder 4.

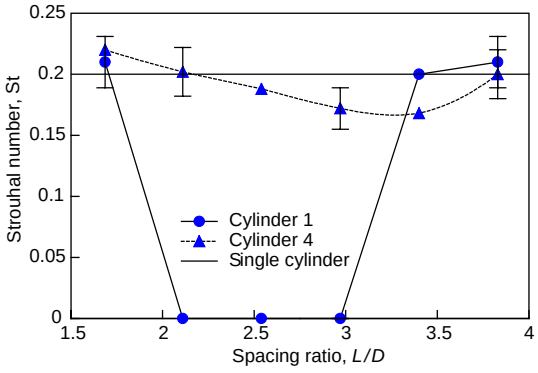

Fig. 7. Variation of St with L/D at $\alpha = 0°$.

shedding started to cease for cylinders 1 and 2 at $L/D<3.94$. This is due to the difference in technique used to measure shedding frequency (counting of shed vortices vs. spectral analysis of the measured fluctuating forces) and a difference in Re. It should be noted that for an in-line square arrangement, it might not be correct to directly relate the indirect method of counting vortex-shedding frequencies to the direct measurement of fluctuating forces on cylinders. Due to the 'shielding flow pattern', counting has to be carried out behind the downstream cylinder while the free shear layers are actually developed from the upstream cylinder. Further comparison of the flow pattern shown in Lam and Lo (1992) with the present flow visualization revealed that the force measurement results highlight the dependence of vortex shedding characteristics on the change of flow patterns.

The force measurement results are presented in Fig. 8. Generally, the fluctuating lift and drag force coefficient, C'_L and C'_D, respectively, of cylinder 4 are more than double that of cylinder 1, thus showing the significant effect of vortex shedding behind the downstream cylinders and the stabilizing effect of shielding flow on the upstream cylinder. Also, the magnitude of C'_L is about double that of C'_D for all L/D tested. It is interesting to note that both C'_L and C'_D drop rapidly as L/D decreases from 3.83 to 3.4 for cylinder 4. This location might correspond to the transition of flow pattern from a vortex shedding flow to a shear layer attachment flow. On the other hand, during the fully shielded flow of cylinder 1 in the range of $L/D=1.69$–2.54, the variation of the fluctuating forces is milder.

As for the mean forces, the mean drag coefficient C_D of cylinder 4 becomes negative at $L/D=2.11$, which is in good agreement with the results of Lam and Fang (1995). Furthermore, the C_D of cylinder 1 rises gradually while the C_D of cylinder 4 drops smoothly as L/D decreases. In contrast, the mean lift coefficient C_L for both cylinders 1 and 4 are negative and the magnitudes decrease swiftly at $L/D<2.97$. This negative behavior is expected and shows that the top and bottom cylinders are repelling each other. These results further show that interference between the two rows of side-by-side cylinders becomes more severe as L/D decreases. At $L/D=1.254$, it was observed that a bi-stable flow occurs for the instrumented cylinder at $\beta=135^\circ$, which corresponds to the position of cylinder 4 at $\alpha=0^\circ$ with $\mathrm{Re}=4.5\times10^4$. The history of the signals measured on cylinder 4 for such bi-stable flow (similar to that reported by Lam and Lo, 1992) is shown in Fig. 9. It is obvious that the transition of the lift, drag and flow-induced vibration took place at the same time. In this study, it was observed that the length of time between transitions appeared random and unpredictable.

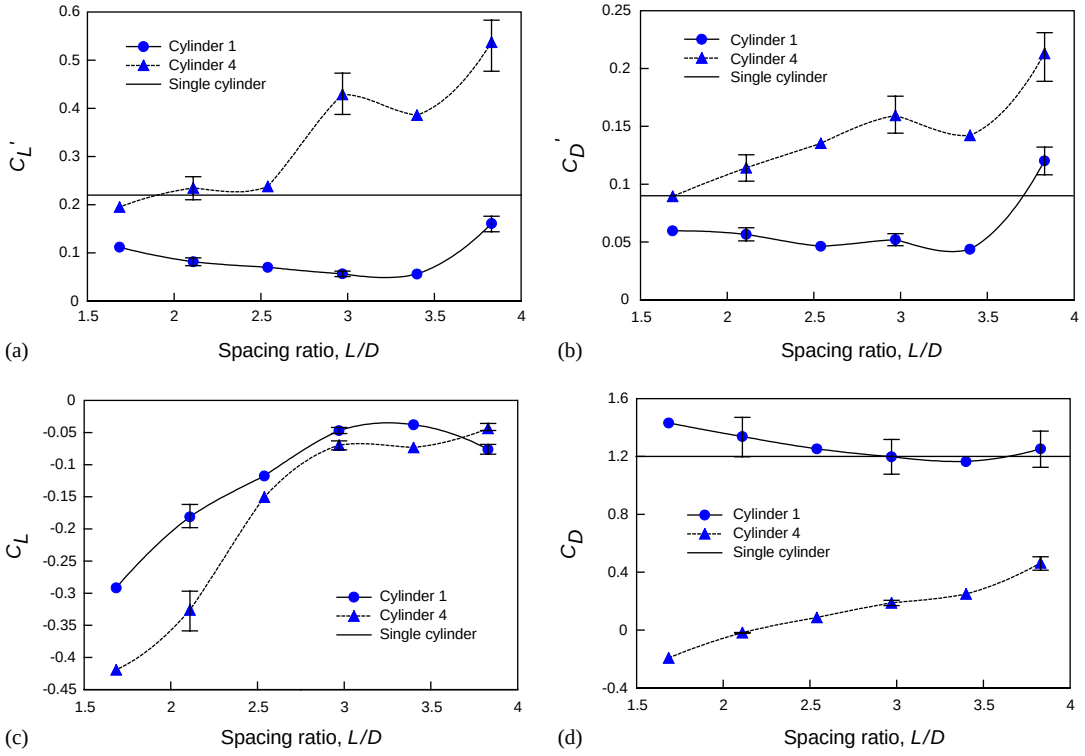

Fig. 8. Variation of force coefficients with L/D at $\alpha=0^\circ$: (a) fluctuating lift force coefficient; (b) fluctuating drag force coefficient; (c) mean lift force coefficient and (d) mean drag force coefficient.

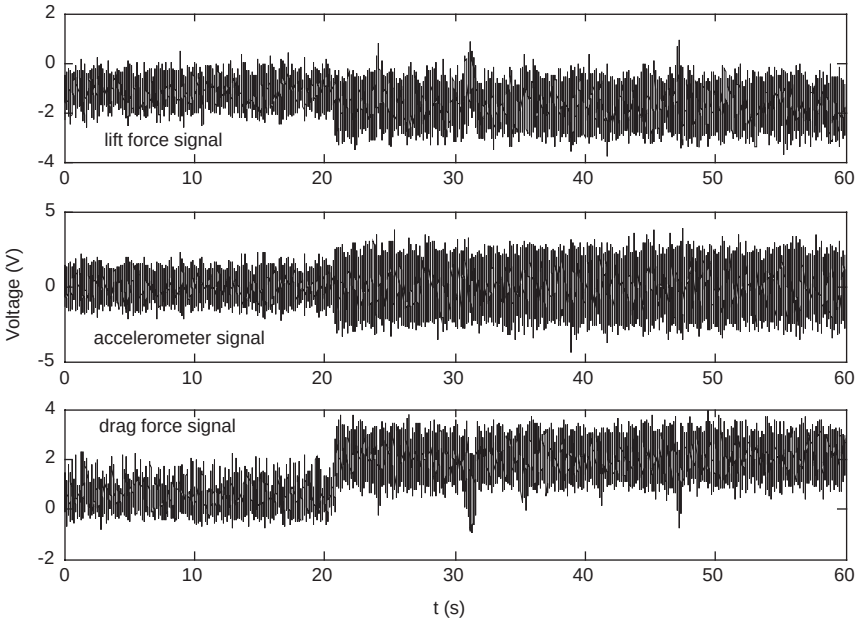

Fig. 9. Time history of force and accelerometer signals of cylinder 4 at $\alpha = 0^\circ$ and $L/D = 1.254$.

3.2. Small staggered angle

Fig. 10 shows the flow visualization result at $\alpha = 15^\circ$ for $\mathrm{Re} = 200$ and 800 in a water tunnel. At this configuration, cylinders 3 and 4 rotate to a lower position compared with cylinders 1 and 2, therefore, the influences of cylinder 2 on cylinder 3, and cylinder 1 on cylinder 4 would be more severe at large spacing ratio. Cylinders 3 and 4 were partially immersed in the wake of the upstream cylinders, therefore, they would experience impingement of the bypassing vortex and an oscillating jet flow above their upper surface. Just as discussed in Lam et al. (2002), it was expected that this would give rise to very strong fluctuating forces on the downstream cylinders and the forces on cylinder 3 would be the highest. Meanwhile cylinders 3 and 4 would exhibit a second or even a third mode harmonic shedding frequency.

The behavior of St shown in Fig. 11 for this configuration is quite different from that of in-line square configuration (c/f with Fig. 7). At $L/D = 3.83$ and 3.4, the peak of the shedding frequency in the spectra is very distinct, and there are additional second and third harmonic frequency for cylinders 3 and 4. However, at $L/D = 2.97$, where a flow pattern of reattachment of the lower shear layers on the downstream cylinders occurs, several peaks appear in the PSD spectrum of the upstream cylinders. A comparison of the results of the PSD plots for the upstream cylinders at $L/D = 3.83$ and 2.97 is shown in Fig. 12. The multiple peaks could be partly attributed to the effects of unsteady attachment of shear layer and the irregularity of vortex shedding. Furthermore, at $L/D = 2.97$, no higher harmonics occurs for cylinders 3 and 4. It is interesting to note that the dominant shedding frequency only appears in the spectrum as a bulge or somewhat wide and flat peak rather than the commonly observed sharp peak. Decreasing L/D further leads to weaker and weaker peaks in the dominant shedding frequency for all cylinders. Therefore, the vortex shedding characteristics could only be identified by carefully studying the shift of the shedding frequency in the spectrum with the change of oncoming velocity, and this is true especially for the downstream cylinders.

The mean and root mean square forces of the four cylinders are shown in Fig. 13. It is obvious that the fluctuating lift and drag forces are very large at $L/D = 3.83$ and 3.4 ($C'_L \approx 0.65$ and $C'_D \approx 0.3$). The reason has been explained in detail by Lam et al. (2002). When L/D decreases to an intermediate value, the lower shear layer of cylinders 1 and 2 would reattach on cylinders 3 and 4. The smaller the L/D, the weaker the oscillation of the shear layer of the upstream cylinders, and this leads to the fluctuating forces on all cylinders to drop swiftly. Therefore, C'_L and C'_D decrease sharply at $L/D = 2.97$. A similar, albeit much milder, drop is also noticed for C_D for cylinders 3 and 4. However, there was a large increase in C_L for cylinder 4 in the L/D range of 2.11–2.97. Lam and Fang (1995) also detected a similar rise in C_L for cylinder 4 in the same L/D range. The rise of C_L could be explained as follows. In the first place, cylinder 4 is partially immersed in the nearly stationary wake of cylinder 1, which has a lower pressure. Secondly, the gap between

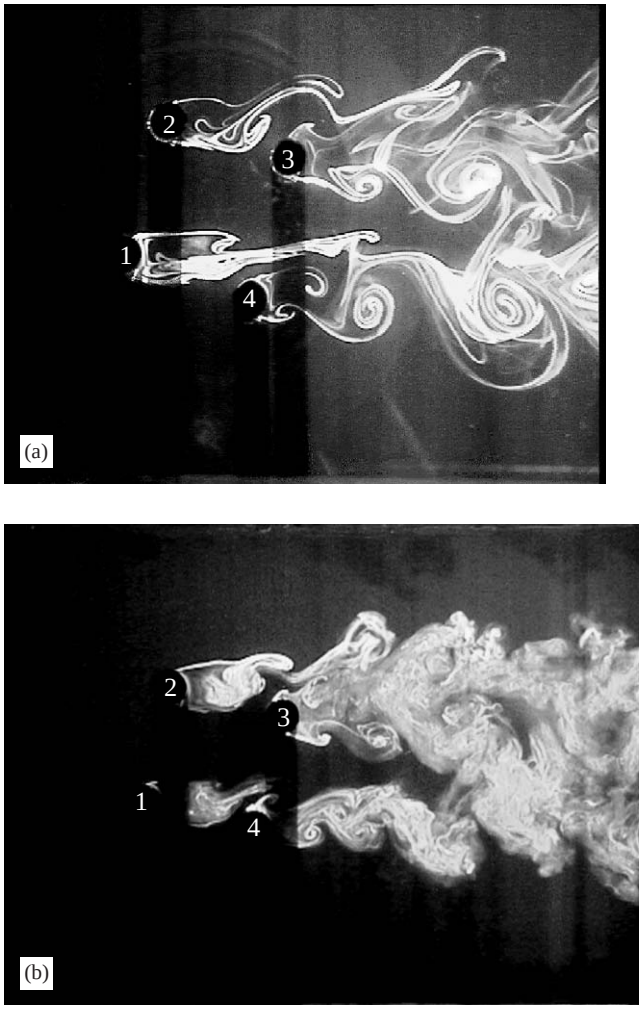

Fig. 10. Typical flow pattern at $\alpha = 15^\circ$ and $L/D = 4$ in a water tunnel: (a) Re = 200 and (b) Re = 800.

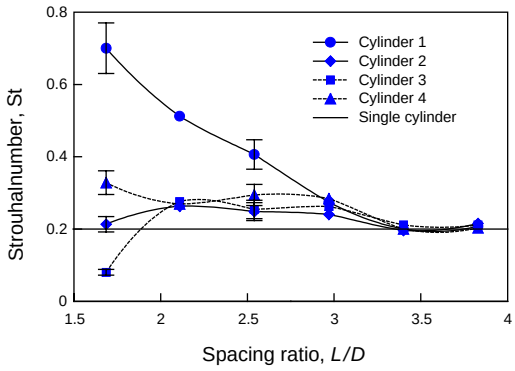

Fig. 11. Variation of St with L/D at $\alpha = 15^\circ$.

cylinders 3 and 4 is large enough not to exert a significant downward lift force on cylinder 4. Although cylinder 3 is also immersed in the wake of cylinder 2, however, the stagnation pressure in the gap flow just under cylinder 3 is low because it is the pressure of the wake of cylinder 1, so C_L of cylinder 3 is not as large as that of cylinder 4.

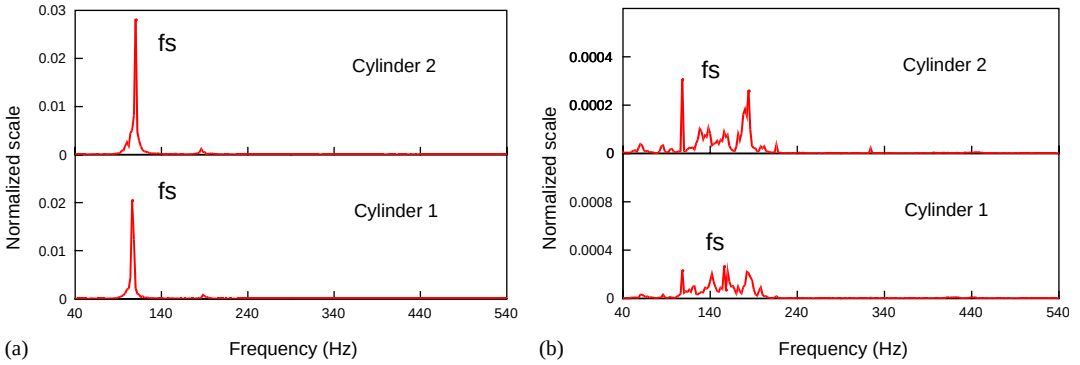

Fig. 12. Power spectral density (PSD) of the lift force vs. frequency at $\alpha = 15°$: (a) PSD of cylinder 1 and 2 at $L/D = 3.83$ and (b) PSD of cylinder 1 and 2 at $L/D = 2.97$.

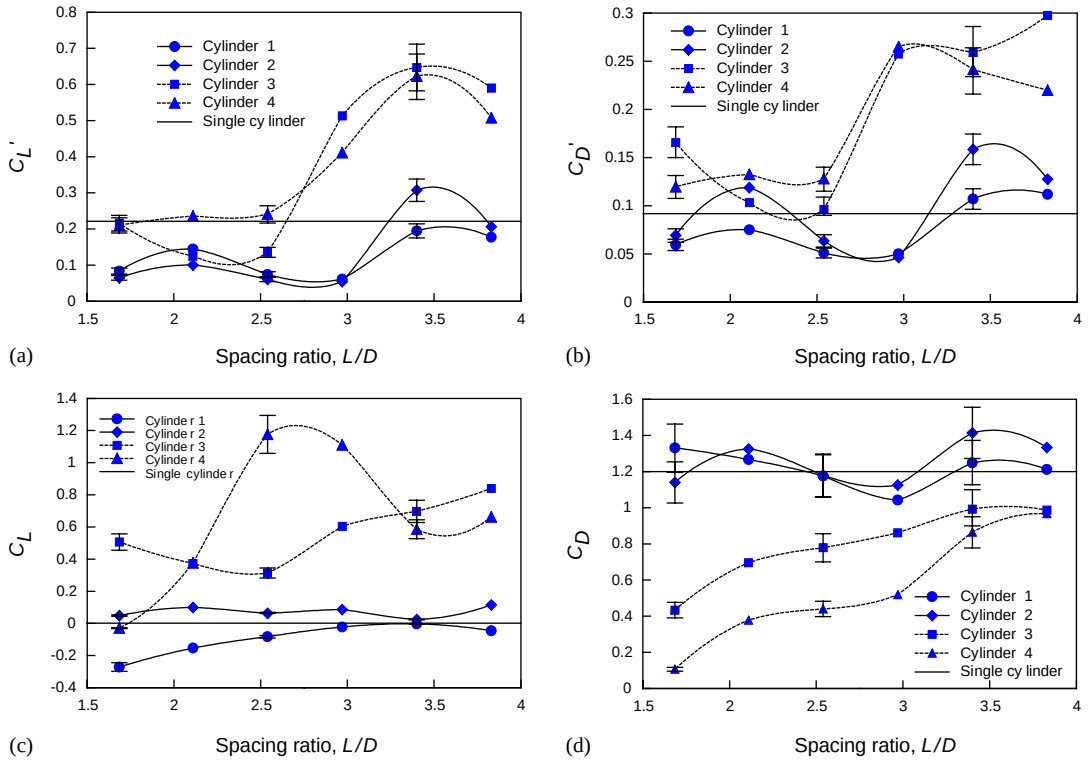

Fig. 13. Variation of force coefficients with L/D at $\alpha = 15°$: (a) fluctuating lift force coefficient; (b) fluctuating drag force coefficient; (c) mean lift force coefficient and (d) mean drag force coefficient.

3.3. Large staggered angle

With α increases to 30°, cylinders 1 and 3 are almost uniformly located between cylinders 2 and 4. The general flow pattern at this configuration is presented in Fig. 14 for Re = 200 and 800. Therefore, at large L/D, all four cylinders together behave like a single cylinder. When L/D is decreased to the upper intermediate limit, the interference would become almost equally severe. This feature is quite different from the interference observed at $\alpha = 0°$ and 15°, which shows a dominant interference between two cylinders in tandem or staggered. Since cylinder 3 is located downstream of cylinders 1 and 2, it would experience a strong interference effect. Similar to that at $\alpha = 15°$, an oscillating jet flow or a

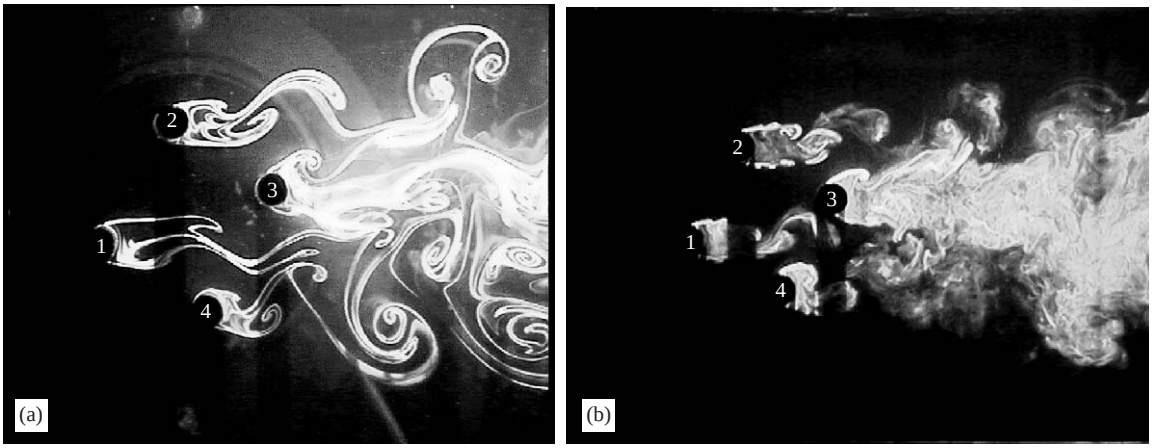

Fig. 14. Typical flow pattern at $\alpha = 30^\circ$ and $L/D = 4$ in a water tunnel: (a) Re = 200 and (b) Re = 800.

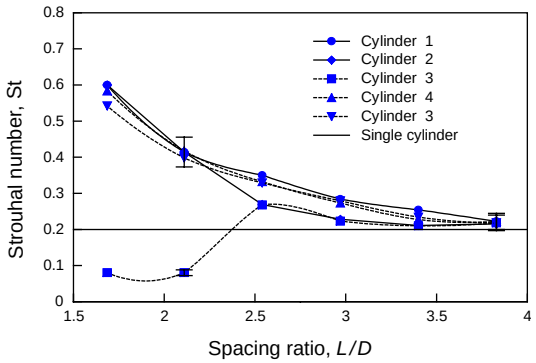

Fig. 15. Variation of St with L/D at $\alpha = 30^\circ$.

bypassing vortex could form near cylinder 3, and its influence on the fluctuating lift forces on cylinder 3 becomes severe only at a relatively small L/D. This means that a narrower jet with higher oscillating frequency has formed. As L/D is reduced further, the oscillation of the wake of cylinder 1 is suppressed more strongly, so is cylinder 2. Therefore, their contributions to the fluctuating lift force on cylinder 3 decrease quickly. Cylinder 3 is almost immersed in the wake of cylinders 1 and 2 when $L/D < 2.11$. This leads to a rapid reduction of C_D. On the other hand, since the upper surface of cylinder 4 is immersed in the wake of cylinder 1, its C_L increases rapidly as L/D decreases.

The St vs. L/D plot of the four cylinders is shown in Fig. 15. At $L/D = 3.83$, the St deduced for all four cylinders are essentially identical. Its value is slightly higher than that obtained for a single cylinder. The largest difference in the measured St at $L/D = 3.83$ is about 8%, which means that the interference at this L/D is weak. At $L/D = 3.4$, two distinct frequencies can be identified for all four cylinders, much like the case for a single cylinder. However, at $L/D = 2.97$, only cylinders 1 and 3 show two distinct frequencies with a slightly higher value for cylinder 1. On reducing L/D further, no cylinder except cylinder 3 yields a discernible second frequency. In Fig. 15, it is of interest to note that one of the two curves of St for cylinder 3 is close to that for cylinder 2, while the other curve is close to that of cylinders 1 and 4. This implies that interference among the cylinders is quite strong.

The variation of the measured forces with L/D at $\alpha = 30^\circ$ is presented in Fig. 16. The fluctuating lift force for cylinder 3 reaches its maximum ($C_L' = 0.52$) at L/D=2.97. In contrast, a maximum of $C_L' = 0.65$ is found at $L/D = 3.4$ for $\alpha = 15^\circ$. The shift of the maximum C_L' location from a large L/D to a small one with increasing α is caused by the formation of oscillating narrow jet flow. The reduction of the maximum value is most likely caused by a decrease of the oncoming flow velocity between cylinders 1 and 2 at smaller L/D (or frontal area). Therefore, it can be said that the oscillating jet flow is an important mechanism governing flow-induced vibration of cylinder arrays. Another interesting observation is that, with decreasing L/D, C_L for cylinder 4 rises from $C_L = 0.13$ at $L/D = 3.83$ almost steadily

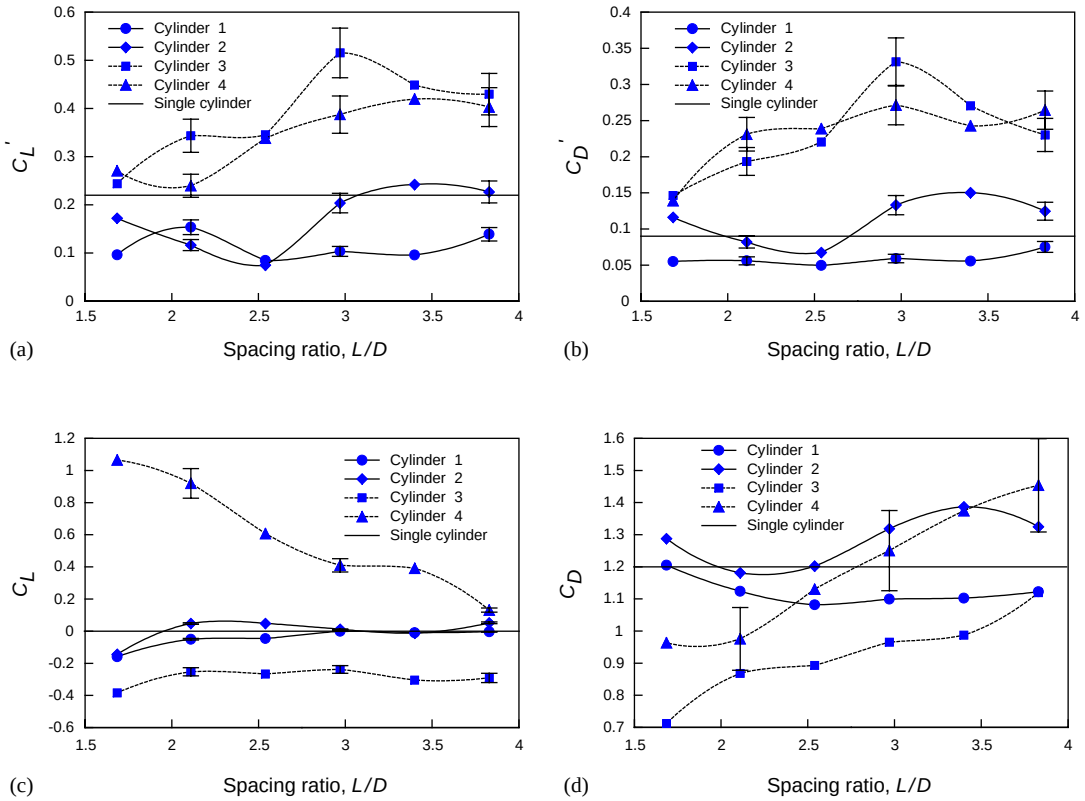

Fig. 16. Variation of force coefficients with L/D at $\alpha = 30°$: (a) fluctuating lift force coefficient; (b) fluctuating drag force coefficient; (c) mean lift force coefficient and (d) mean drag force coefficient.

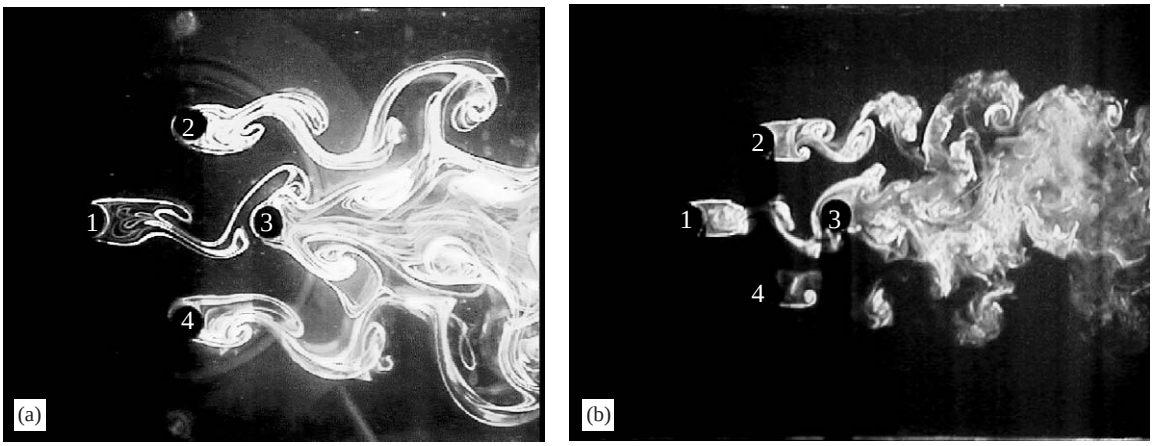

Fig. 17. Typical flow pattern at $\alpha = 45°$ and $L/D = 4$ in a water tunnel: (a) Re = 200 and (b) Re = 800.

to $C_L = 1.06$ at $L/D = 1.69$ with a step appearance at $L/D = 2.97$– 3.4. This variation agrees quite well with the results of Lam and Fang (1995). From the present observation on flow patterns and their comparison with those of Lam and Lo (1992), a possible explanation could be put forward. At $L/D > 1.69$, the shedding vortices from cylinder 1 always impinge on the lower half surface of cylinder 3 and entrain into the gap between cylinders 3 and 4. Thus, lower pressure region is formed under cylinder 3; while a relative strong gap flow with a high velocity and a high stagnation pressure passes over the upper half of cylinder 3. This gives rise to a negative lift force on cylinder 3. Due to the low-pressure region between cylinders 3 and 4, the lift force on cylinder 4 is always positive and increases to high values at small L/D.

3.4. Rotated square array

At $\alpha = 45°$, this array gives a rotated square configuration. As the arrangement is symmetrical, only the results for cylinders 1–3 are shown here. A general flow pattern at this α for $Re = 200$ and 800 is shown in Fig. 17. It can be seen that at a large L/D, cylinder 3 is impinged continuously by the shed vortices from cylinder 1 because cylinder 3 is located directly downstream of cylinder 1. Hence, C_L' becomes rather large compared with that for a single cylinder. In the range of intermediate to upper intermediate L/D, a rather interesting interference phenomenon occurs, i.e., the fluctuating forces of all three cylinders show two prominent frequencies. In the study of Lam and Lo (1992), they found that, in the flow patterns for $L/D > 2.4$, the wake of cylinder 1 is comparatively narrow. This is due to the gap flow on

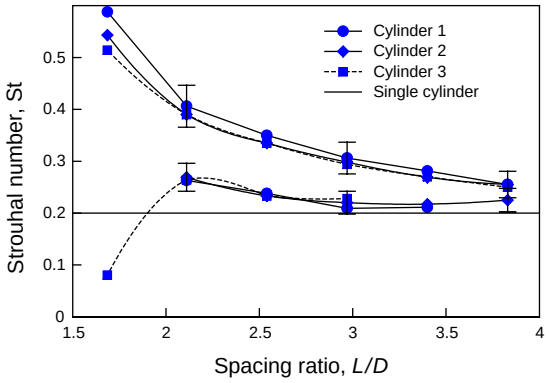

Fig. 18. Variation of St with L/D at $\alpha = 45°$.

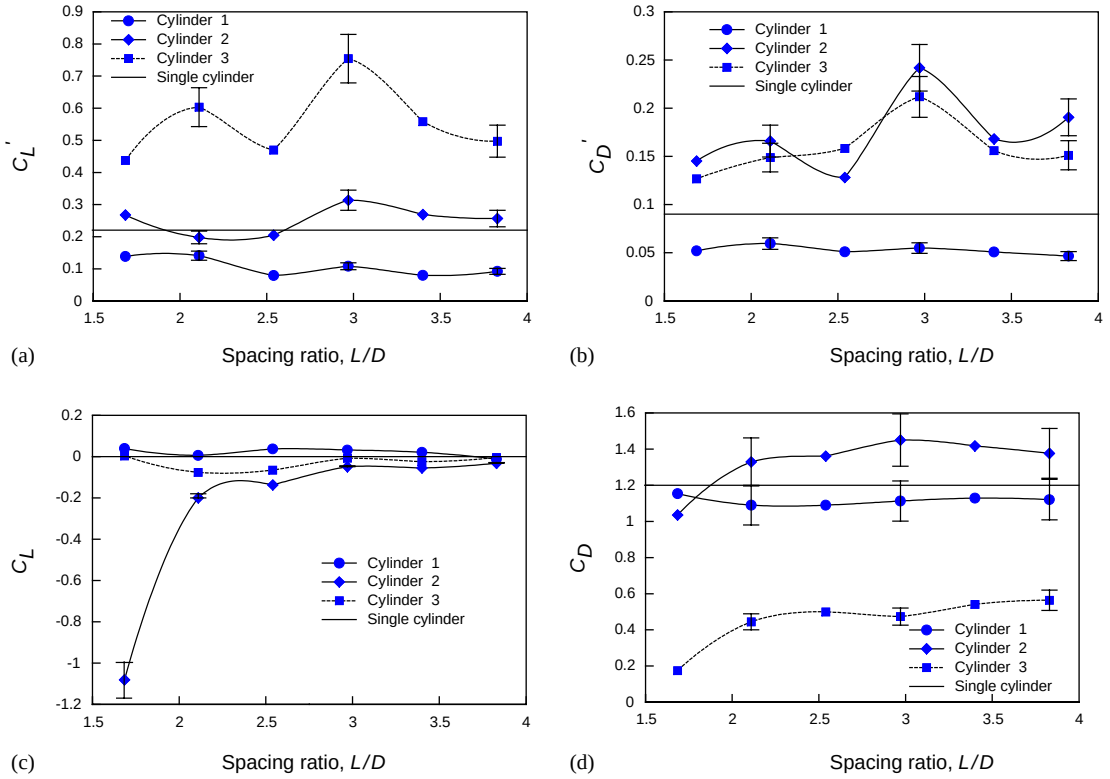

Fig. 19. Variation of force coefficients with L/D at $\alpha = 45°$: (a) fluctuating lift force coefficient; (b) fluctuating drag force coefficient; (c) mean lift force coefficient and (d) mean drag force coefficient.

each side rushing into the central region and the suppression of natural expansion of the shear layers in the transverse direction after separation is restricted. Despite the wake being sandwiched between the gap flow it is not always stable and stays in place in the middle. Sometimes the wake might be biased upward or downward. It is believed that the instability of the wake of cylinder 1 and its shift are the cause of two dominant frequencies observed in every cylinder. On the other hand, the C_L' on cylinder 3 would gradually increase until it reaches its maximum, at which point the contributions to the fluctuating lift force of the oncoming vortices and the disturbed gap flow on both sides of cylinder 3 are rather large. Reducing further L/D to <1.69, vortex shedding from cylinder 1 disappeared, but vortex shedding from cylinder 2 still exists even though its strength decreases quickly.

The St vs. L/D plot is shown in Fig. 18. A second branch of St for cylinder 1 appears in the range of L/D=2.11–3.4, while that for cylinder 2 shows up at L/D=2.11–3.83 and for cylinder 3 at L/D=1.69–2.97. The result shows that the St values for cylinder 1 and 2 increase sharply as L/D drops below 2.54; while there is a sudden drop of St value for cylinder 3 below L/D=2.11. Examining the figure more closely, it is noticed that in the range L/D=2.1–2.97, St has two distinctive branches. The difference between the two branches becomes larger with decreasing L/D.

The variation of forces with L/D at $\alpha = 45^\circ$ are shown in Fig. 19. In Fig. 19(a), it is interesting to note that the fluctuating lift force for cylinder 3 at $L/D = 3.83$ are given by $C_L' = 0.5$ and $C_D' = 0.15$, which are almost equal to those for cylinder 3 at L/D=3.83 and $\alpha = 0^\circ$. The fluctuating lift force then rises to $C_L' = 0.75$ at $L/D = 2.97$, and this C_L' is the maximum value for all α and L/D examined. As for C_L, there is a sharp jump for cylinder 2 at $L/D = 1.69$, whereas at large L/D, the C_L for every cylinder remains a relatively small value. This can be explained by the fact that the gap flow on each side of cylinder 2 would reach their maximum velocity and tilt angle at the right L/D. Located directly downstream of cylinder 1, the C_D on cylinder 3 is small compared with that of cylinders 1 and 2. It is impossible for cylinder 3 to be completely shielded by cylinder 1 because cylinders 2 and 4 are located on both sides of cylinder 3 and would disturb the flow around it seriously.

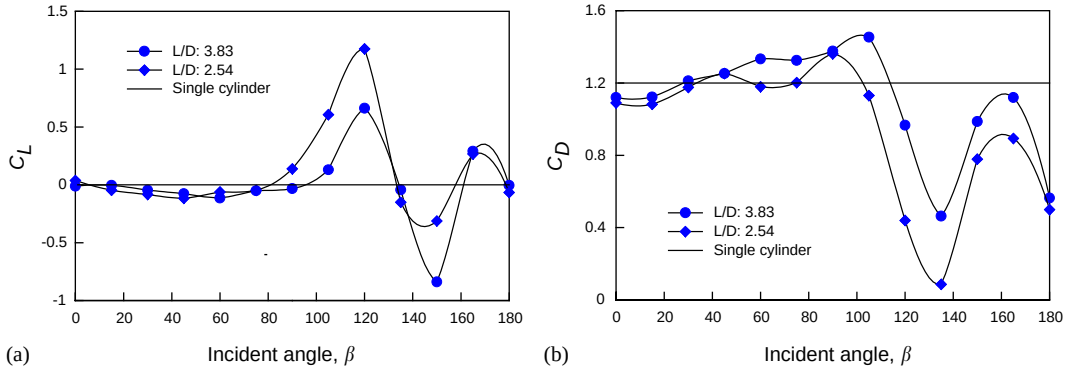

Fig. 20. Variation of mean force coefficients with L/D and β.

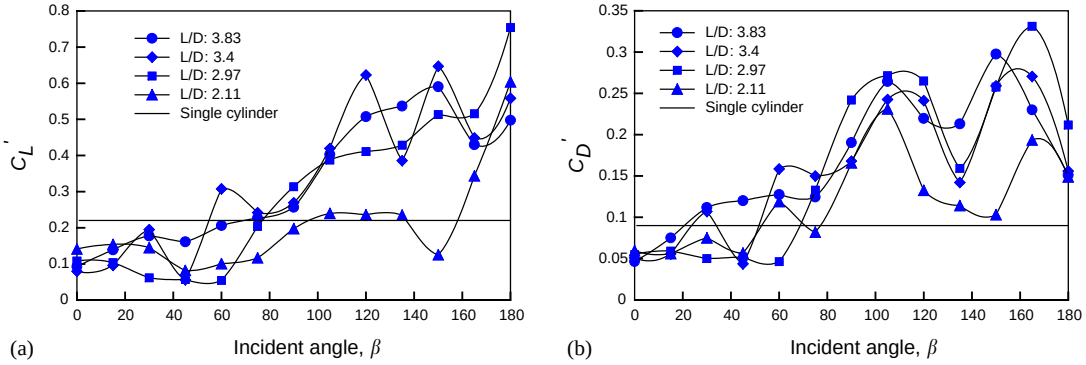

Fig. 21. Variation of fluctuating force coefficients with L/D and β.

3.5. Variation of forces with l/d and β

As a basic element, four-cylinder array in a square configuration has many direct applications in different engineering disciplines. Therefore, it is useful to study the variation of mean forces with β and L/D because rather large unsteady force might arise as a consequence of a sudden change of direction of the oncoming flow. Fig. 20 shows some typical results of C_L and C_D vs. β. The C_L curve for $L/D=3.83$ clearly shows a sharp variation at $\beta=135^\circ$, which corresponds to the location of cylinders 3 or 4 at $\alpha=0^\circ$. Similarly, the C_L curve for L/D=2.54 also shows a rapid variation in the range of $\beta=120-150^\circ$, which is the location of cylinders 3 and 4 at $\alpha=0-15^\circ$. This means that a small change of α at $\alpha=\pm0-15^\circ$ could cause large variation of C_L on cylinders 3 or 4. Consequently, in an unsteady flow, the change of direction of the oncoming flow might lead to a fairly substantial variation of the unsteady lift force on cylinders 3 and 4. Another interesting point is to observe the variations of C'_L and C'_D with L/D and β. Four plots of C'_L and C'_D vs. β at different L/D are shown in Fig. 21. At large L/D, such as $L/D=3.83$ and 3.4, maximum C'_L and C'_D occurs at $\beta=150^\circ$ which is the location of cylinder 3 at $\alpha=15^\circ$. However, at $L/D=2.97$, the location where maximum C'_L and C'_D occurs gradually moves to $\beta=165^\circ$ and 180°, and this β corresponds to the position of cylinder 3 at $\alpha=30^\circ$ and 45°, respectively. Further reducing L/D to 2.11, the location of the maximum C'_L and C'_D shifts to $\beta=180^\circ$, which corresponds to the position of cylinder 3 at $\alpha=45^\circ$, with rather small values at other β. As discussed above, the shift of the maximum C'_L and C'_D is closely related to the change of flow patterns. Consequently, for engineering applications, it should be noted that a small change in the oncoming flow direction at $\alpha=\pm0-15^\circ$ contributes significantly to flow-induced vibration on the downstream cylinders. Another important contributor to flow-induced vibration of the downstream cylinders is the oncoming vortex or the formation of an oscillating narrow gap flow, which could give rise to large rms forces on the downstream cylinders and lead to serious consequences.

4. Conclusions

Extensive measurements have been carried out on the mean and fluctuating forces and their associated St of four cylinders in a square arrangement in a cross flow using a piezo-electric load cell. Six different L/D ranging from 3.83 to 1.69 at an interval of 0.43, and 13 different incident angles β ranging from 0° to 180° at an interval of 15°, which correspond to four different array angles $\alpha=0^\circ$, 15°, 30° and 45°, were covered in this investigation. Moreover, four different oncoming velocities, which correspond to $Re=2.25\times10^4$ to 4.5×10^4 based on the oncoming uniform flow and the diameter of the individual cylinder, were conducted for all arrangements. Some useful results are obtained and they are summarized as follows.

(i) The anticipated results, that the upstream cylinders will usually experience larger mean drag force C_D than the downstream ones, while the downstream cylinders are usually subjected to higher fluctuating forces under the influence of unsteady wake vortices, were realized.

(ii) Flow patterns, i.e., the development and the interferences of the free shear layers and the distribution of the wakes of the cylinders play a key role in the variation of forces and their frequencies. Furthermore, flow patterns are the key to understand the results and the behavior of St and the fluctuating forces. Generally, the variation of the forces and St can be divided into three different stages according to L/D at every array angle α, but the range of L/D varies for different α.

(iii) At large L/D, the dominant mechanism on flow-induced vibration is the shear layers and their interference. In general, a dominant frequency is discernible in the PSD force spectrum of every cylinder, and the rms fluctuating forces are greater than those at a smaller L/D.

(iv) At intermediate L/D, the primary mechanism is the almost stationary wakes and their interference on different cylinders. Since the downstream cylinders are completely or partly immersed in the nearly stationary wakes of the upstream ones, a rapid decrease of the root mean square fluctuating forces on the downstream cylinders usually follows. An exception is observed at $\alpha=45^\circ$, where an increase rather than a decrease is recorded.

(v) At small L/D, the four cylinders enclosed a very small region of fluid. Consequently, the gap flow between them would vary greatly with a small change of L/D. This gives rise to a major characteristic; that is, the large variation of mean forces with L/D.

(vi) Two important mechanisms responsible for flow-induced vibration are analyzed and the fluctuating forces have also been measured. The first one is the formation of an oscillating narrow jet flow around the downstream cylinders, the typical results are represented by the C'_L and C'_D values deduced for cylinder 3 at $\alpha=15^\circ$ and at $L/D=3.4$. The second one is the impingement of the oncoming shed vortices on the downstream cylinders. Typical results are indicated by the C'_L and C'_D values of cylinder 3 at $\alpha=0^\circ$ and 45° and at $L/D=3.83$. Furthermore,

under the influence of a combination of the two mechanisms, C'_L and C'_D would increase substantially, such as the C'_L and C'_D of cylinder 3 at $\alpha = 45^\circ$ and $L/D = 2.97$. The change of direction of the oncoming flow is another mechanism that contributes to flow-induced vibration in unsteady flow around cylinders.

Acknowledgements

This work was fully supported by a grant from the Research Grants Council of the Hong Kong Special Administrative Region, Peoples Republic of China, under Project No. PolyU5147/99E.

References

Baban, F., So, R.M.C., 1991a. Recirculating flow behind and unsteady forces on finite-span circular cylinders in a cross-flow. Journal of Fluids and Structures 5, 185–206.

Baban, F., So, R.M.C., 1991b. Aspect ratio effect on flow-induced forces on circular cylinder in a cross-flow. Experiments in Fluids 10, 313–321.

Baban, F., So, R.M.C., Ötugen, M.V., 1989. Unsteady forces on circular cylinders in a cross flow. Experiments in Fluids 7, 293–302.

Blackburn, H.M., Henderson, R.D., 1999. A study of two-dimensional flow past an oscillating cylinder. Journal of Fluid Mechanics 385, 255–286.

Blackburn, H.M., Melbourne, W.H., 1996. The effect of free-stream turbulence on sectional lift forces on a circular cylinder. Journal of Fluid Mechanics 306, 267–292.

Farrant, T., Tan, M., Price, W.G., 2000. A cell boundary element method applied to laminar vortex-shedding from arrays of cylinders in various arrangements. Journal of Fluids and Structures 14, 375–402.

Fitzpatrick, J.A., Donaldson, I.S., Mcknight, W., 1988. Strouhal numbers for flows in deep tube array models. Journal of Fluids and Structures 2, 145–160.

Fox, T.A., West, G.S., 1993a. Fluid-induced loading of cantilevered circular cylinders in a low turbulence uniform flow. Part 1: mean loading with aspect ratios in the range 4–30. Journal of Fluids and Structures 7, 1–14.

Fox, T.A., West, G.S., 1993b. Fluid-induced loading of cantilevered circular cylinders in a low turbulence uniform flow. Part 2: fluctuating loads with aspect ratios in the range 4–30. Journal of Fluids and Structures 7, 15–28.

Fox, T.A., West, G.S., 1993c. Fluid-induced loading of cantilevered circular cylinders in a low turbulence uniform flow. Part 3: fluctuating loads with aspect ratios in the range 4–30. Journal of Fluids and Structures 7, 375–386.

Freitas, C.J., 1995. Perspective: selected benchmarks from commercial CFD codes. ASME Journal of Fluids Engineering 117, 208–218.

Guillaume, D.W., LaRue, J.C., 1999. Investigation of the flopping regime with two-, three- and four-cylinder arrays. Experiments in Fluids 27, 145–156.

Igarashi, T., 1981. Characteristics of the flow around two circular cylinders arranged in tandem (1st Report). Bulletin of the JSME 24, 323–331.

Kareem, A., Kijewski, T., Lu, P.C., 1998. Investigation of interference effects for a group of finite cylinders. Journal of Wind Engineering and Industrial Aerodynamics 77 and 78, 503–520.

Kim, H.J., Durbin, P.A., 1988. Investigation of the flow between a pair of circular cylinders in the flopping regime. Journal of Fluid Mechanics 196, 431–448.

Lam, K., Cheung, W.C., 1988. Phenomena of vortex shedding and flow interference of three cylinders in different equilateral arrangements. Journal of Fluid Mechanics 196, 1–26.

Lam, K., Fang, X., 1995. The effect of interference of four equispaced cylinders in cross flow on pressure and force coefficients. Journal of Fluids and Structures 9, 195–214.

Lam, K., Lo, S.C., 1992. A visualization study of cross-flow around four cylinders in a square configuration. Journal of Fluids and Structures 6, 109–131.

Lam, K., Li, J.Y., So, R.M.C., 2001. Flow around four cylinders in a square configuration using surface vorticity method. In: Ünal, M.F. (Ed.), Proceeding of the Second International Conference on Vortex Methods, Istanbul, Turkey, September 26–28, 2001.

Lam, K., Li, J.Y., Chan, K.T., So, R.M.C., 2003. Flow pattern and velocity field distribution of cross-flow around four cylinders in a square configuration at a low Reynolds number. Journal of Fluids and Structures 17, 665–679.

Li, J., Sun, J., Roux, B., 1992. Numerical study of an oscillating cylinder in uniform flow and in the wake of an upstream cylinder. Journal of Fluid Mechanics 237, 457–478.

Newman, D.J., Karniadakis, G.E., 1997. A direct numerical simulation study of flow past a freely vibrating cable. Journal of Fluid Mechanics 344, 95–136.

Oengoren, A., Ziada, S., 1998. An in-depth study of vortex shedding, acoustic resonance and turbulent forces in normal triangle tube arrays. Journal of Fluids and Structures 12, 717–758.

Paidoussis, M.P., 1982. A review of flow-induced vibrations in reactors and reactor components. Nuclear Engineering and Design 74, 31–60.

Price, S.J., Paidoussis, M.P., 1984. The aerodynamic forces acting on groups of two and three circular cylinders when subjected to a cross-flow. Journal of Wind Engineering and Industrial Aerodynamics 17, 329–347.

Price, S.J., Zahn, M.L., 1991. Fluidelastic behavior of a normal triangular array subject to cross-flow. Journal of Fluids and Structures 5, 259–278.

Richter, A., Naudascher, E., 1976. Fluctuating forces on a rigid circular cylinder in confined flow. Journal of Fluid Mechanics 78, 561–576.

Sakamoto, H., Haniu, H., 1994. Optimum suppression of fluid forces acting on a circular cylinder. ASME Journal of Fluids Engineering 116, 221–227.

Sayers, A.T., 1988. Flow interference between four equispaced cylinders when subjected to a cross flow. Journal of Wind Engineering and Industrial Aerodynamics 31, 9–28.

Sayers, A.T., 1990. Vertex shedding from groups of three and four equispaced cylinders situated in a cross flow. Journal of Wind Engineering and Industrial Aerodynamics 34, 213–221.

Schewe, G., 1983. On the force fluctuations acting on a circular cylinder in crossflow from subcritical up to transcritical Reynolds numbers. Journal of Fluid Mechanics 133, 265–285.

Sin, V.K., So, R.M.C., 1987. Local force measurement on finite-span cylinders in a cross-flow. ASME Journal of Fluids Engineering 109, 136–143.

So, R.M.C., Savkar, S.D., 1981. Buffeting forces on rigid circular cylinders in cross flows. Journal of Fluids Mechanics 105, 397–425.

So, R.M.C., Liu, Y., Chan, S.T., Lam, K., 2001. Numerical studies of a freely vibrating cylinder in a cross-flow. Journal of Fluids and Structures 15, 845–866.

Sumner, D., Wong, S.S.T., Price, S.J., Paidoussis, M.P., 1999. Fluid behaviour of side-by-side circular cylinders in steady cross-flow. Journal of Fluids and Structures 13, 309–338.

Sumner, D., Price, S.J., Paidoussis, M.P., 2000. Flow-pattern indentification for two staggered circular cylinders in cross flow. Journal of Fluid Mechanics 411, 263–303.

Szepessy, S., Bearman, P.W., 1992. Aspect ratio and end plate effects on vortex shedding from a circular cylinder. Journal of Fluid Mechanics 234, 191–217.

Tadrist, H., Martin, R., Tadrist, L., 1990. Experimental investigation of fluctuating forces exerted on a cylindrical tube (Reynolds numbers from 3000 to 30 000). Physics of Fluids A 2 (12), 2176–2182.

Ting, D.S.-K., Wang, D.J., Price, S.J., Paidoussis, M.P., 1998. An experimental study on the fluidelastic forces for two staggered cylinders in cross flow. Journal of Fluids and Structures 12, 259–294.

Tutar, M., Hold, A.E., 2001. Computational modeling of flow around a circular cylinder in subcritical flow regime with various turbulence models. International Journal for Numerical Methods in Fluids 35, 763–784.

West, G.S., Apelt, C.J., 1982. The effects of tunnel blockage and aspect ratio on the mean flow past a circular cylinder with Reynolds numbers between 10^4 and 10^5. Journal of Fluid Mechanics 114, 361–377.

West, G.S., Apelt, C.J., 1993. Measurements of fluctuating pressures and forces on a circular cylinder in the Reynolds number range 10^4 to 2.5×10^5. Journal of Fluids and Structures 7, 227–244.

West, G.S., Apelt, C.J., 1997. Fluctuating lift and drag forces on finite length of a circular cylinder in the subcritical Reynolds number range. Journal of Fluids and Structures 11, 135–158.

Zdravkovich, M.M., 1987. The effects of interference between circular cylinders in cross flow. Journal of Fluids and Structures 1, 239–261.